Desalination and Water Treatment
www.deswater.com

doi: 10.5004/dwt.2023.30072

313 (2023) 162–172
November

Preparation and adsorption study of polyvinyl alcohol-functionalized sodium alginate composite hydrogel for Pb(II) in aqueous solutions

Huiling Zhang[a,b,*], Ziyan Ye[a,b], Junjie Liang[a], Zekang Hu[a], Hongyu Liu[a]

[a]*School of Resource and Environmental Engineering, Wuhan University of Science and Technology, Wuhan 430081, China, emails: zhanghuiling@wust.edu.cn (H. Zhang), yeziyan0330@wust.edu.cn (Z. Ye), renzhuang0619@163.com (J. Liang), wkd5409@163.com (Z. Hu), liuhongyu5409@163.com (H. Liu)*
[b]*National Environmental Protection Key Laboratory of Mineral and Metallurgical Resource Utilization and Pollution Control, Wuhan University of Science and Technology, Wuhan 430081, China*

Received 16 June 2023; Accepted 3 October 2023

ABSTRACT

This paper presents the utilization of sodium alginate (SA) as a raw material to construct a double network structure through the incorporation of chitosan (CS) and the electrostatic polymerization of SA. Subsequently, by employing polyvinyl alcohol (PVA) as a functional material, a modified SA/CS/PVA composite hydrogel (SCPH) was prepared via the Ca(II) ion exchange method. The hydrogel exhibited a flocculent form, thereby greatly enhancing the removal of Pb(II). The adsorption process of Pb(II) by the SCPH reached equilibrium within 30 min, achieving a remarkable removal rate of 97.45% and a maximum adsorption capacity of 147.93 mg/g (298 K). A series of characterization analyses have been employed to investigate the structure and adsorption mechanism of hydrogels, and the adsorption mechanism involves ion exchange, electrostatic attraction, as well as the complexation of hydroxyl and carboxyl groups. Batch adsorption experiments were conducted at different temperatures and pH levels, and the kinetics and isotherms were investigated. The Langmuir isotherm and pseudo-second-order kinetic model were found to best fit the experimental data, suggesting the feasibility of using the SCPH as an efficient adsorbent for Pb(II) removal. Moreover, the dual network structure constructed by SA and CS significantly enhances the adsorption performance of SCPH. At the same time, PVA strengthens the mechanical strength of SCPH, which is favorable for recycling. As a low-cost and efficient adsorbent, SCPH can be widely used in water treatment.

Keywords: Sodium alginate; Composite hydrogel; Pb(II); Adsorption mechanism

1. Introduction

The rapid advancement of China's social economy has raised a pressing concern: the escalation of water pollution. The quality of water environments is significantly compromised by wastewater discharge, primarily from industrial sectors such as metallurgy, electroplating, paper making, printing and dyeing, and tanneries [1,2]. Within these industries, lead ions (Pb(II)) emerge as one of the most harmful pollutants, possessing a range of hazardous properties, including carcinogenicity, bioaccumulation, non-biodegradability, and toxicity [3]. Exposure to or ingesting lead can lead to severe damage to vital bodily systems and is even associated with the development of cancer [4]. Consequently, the removal of Pb(II) from wastewater assumes paramount importance [5]. Notable examples include electrolytic membrane filtration, chemical precipitation [6], and coagulation [7]. However, these technologies have limitations, as they often exhibit suboptimal performance, high operating costs, and the potential for secondary pollution. In contrast, adsorption has emerged as a highly promising approach due

* Corresponding author.

to its inherent advantages. This method offers simplicity of operation [8], cost-effectiveness [9], and the absence of contamination by-products [10,11]. Consequently, adsorption has garnered significant attention and extensively studied [12,13]. The advantages of adsorption make it an appealing choice for addressing the challenges associated with wastewater treatment. By capitalizing on the benefits of adsorption, researchers and practitioners can continue to advance this technology, refining its efficiency, exploring new adsorbents, and expanding its range of applications.

Numerous studies have demonstrated the abundant availability, cost-effectiveness, and remarkable adsorption capabilities of naturally occurring organic molecules, including sodium alginate, chitosan, cellulose, and gelatine, for mitigating environmental pollutants [14]. Among these, sodium alginate (SA), as a natural anionic polysaccharide polymer, has garnered significant attention owing to its wide array of sources, economical production, excellent biocompatibility, and remarkable heavy metal chelation abilities [15]. SA represents a polyanionic electrolyte containing an anionic carboxyl group. Due to its electrostatic interaction capabilities, SA readily forms polyelectrolyte complexes with polycationic materials, a phenomenon called polyelectrolyte recombination [16]. Notably, the combination of SA with chitosan (CS) results in the formation of a pH-sensitive hydrogel exhibiting chelating adsorption properties, thereby displaying immense potential as a carrier for substance delivery systems [17]. To amplify the adsorption capacity of sodium alginate hydrogels, the prevailing approach involves the fabrication of hydrogel composites through graft copolymerization and electrostatic compounding, utilizing SA as the foundational matrix material [18,19]. These composite materials not only harness the inherent characteristics of natural organic molecules but also demonstrate excellent biocompatibility and minimal environmental and organismal impact during the treatment of contaminated water samples [20]. Consequently, elucidating the adsorption properties and mechanisms of these natural organic molecular adsorbents holds broad industrial implications and offers valuable guidance for practical pollutant remediation endeavours.

A novel approach utilizing a composite hydrogel for the synthesis of cost-effective and environmentally friendly adsorbents is investigated in this study. The functionalizing of SA, CS, and polyvinyl alcohol (PVA) is explored to fabricate SA/CS/PVA composite hydrogel (SCPH) with enhanced efficacy in removing Pb(II) from aqueous solutions. CS is employed to modify SA/CS composites, serving as a precursor material for the fabrication of SCPH. The hydrogels' ion exchange and electrostatic attraction properties are achieved by cross-linking the materials with $CaCl_2$ as a cross-linking agent. Comprehensive characterization techniques, including adsorption experiments, temperature and pH variations, adsorption kinetics, isotherms, and mechanism analysis, were conducted to evaluate the removal mechanism of Pb(II) by SCPH. The scanning electron microscopy coupled with energy-dispersive X-ray spectroscopy (SEM-EDX), Fourier-transform infrared spectroscopy (FTIR), X-ray diffraction (XRD) and X-ray photoelectron spectroscopy (XPS) are employed for further research. This investigation introduces a novel adsorbent characterized by outstanding and consistent adsorption capabilities. Distinguishing itself from conventional SA-type hydrogels, this hydrogel amalgamates the amino group from CS with the hydroxyl group from PVA. It removes pollutants with good effect and low cost so that they can be widely used to treat natural heavy metal ion wastewater.

2. Materials and methods

2.1. Chemical and reagents

Analytically pure reagents, including sodium alginate (SA), polyvinyl alcohol (PVA) (1,750 ± 50), chitosan [CS, $(C_6H_{11}NO_4)_n$], acetic acid (CH_3COOH), anhydrous calcium chloride ($CaCl_2$), anhydrous ethanol, lead nitrate, nitric acid (HNO_3) and sodium hydroxide (NaOH) sourced from China National Pharmaceutical Group Chemical Reagent Co., Ltd., (China).

2.2. Synthesis of SA hydrogel, SA/CS hydrogel, SCPH

- To synthesize the SA hydrogel (SH), 3.0 g of SA was dissolved and gradually added to a 300 mL $CaCl_2$ solution (5% w/v). Under constant temperature, continue to stir the mixture and allow it to solidify for 12 h.
- To create the SA/CS hydrogel (SCH), 3.0 g of SA was incorporated into a solution of CS. The obtained mixture was dissolved and then uniformly added drop by drop into a 300 mL solution of $CaCl_2$ (5% w/v). Stirring the solution consistently at a constant temperature facilitated solidification, which occurred over, for 12 h.
- To prepare the SA/CS/PVA composite hydrogel (SCPH), dissolve 2.0 g of PVA solid in water. This PVA solution was then mixed with the SCH. The obtained mixture should be uniformly dropped into a 300 mL solution of $CaCl_2$ (5% w/v), while continuously stirring at a constant temperature and speed. The mixture formed a flocculent hydrogel, which was left to solidify for 12 h.

2.3. Characterization

The morphology of the sample was analyzed by scanning electron microscope using a Czech TESCAN MIRA LMS. The sample's elemental composition was determined by energy-dispersive X-ray spectroscopy using an AZtec Ultim Live 100 X [Manufactured by Oxford Instruments Technology (Shanghai, China)]. FTIR was performed using the INVENIO R Spectrophotometer (Bruker Group in Karlsruhe, Germany). The crystal structure was studied using the SmartLab SE X-ray Diffractometer (XRD) (Bruker Group in Karlsruhe, Germany). XPS of the hydrogel was obtained using the AXIS Supra+ X-ray photoelectron spectroscopy instrument (Shimadzu (Hong Kong) Ltd.). The zeta potential was measured using the SurPASS Anton Paar zeta potential analyzer. (Malvern Instruments China, situated in Xuhui District, Shanghai, China, is the manufacturer of the "SurPASS Anton Paar zeta potential analyzer")

2.4. Batch adsorption experiments

The SCPH (10–300 mg) was introduced into 50 mL of Pb(II) solution (20–150 mg/L) at pH 1–5. The pH was adjusted using 0.1 M HNO_3 and NaOH solutions, and the adsorption process was conducted under different temperatures (293–323 K) for various durations. To investigate the adsorption kinetics,

0.5 g of the SCPH was used to adsorb a 50 mL Pb(II) solution with an initial concentration of 150 mg/L, at pH 4, with an oscillation time ranging from 0 to 70 min. The adsorption isotherms were constructed by varying the initial Pb(II) solution concentration (20–150 mg/L) at a temperature of 298 K and a pH of 4. The equilibrium adsorption capacity (Q_t, mg/g) and removal rate (R %) were determined using Eqs. (1) and (2):

$$Q_t = \frac{(C_0 - C_t)}{m} \times V \quad (1)$$

$$R = \frac{(C_0 - C_t)}{C_0} \times 100\% \quad (2)$$

The initial concentration of pollutants is denoted as C_0 (mg/L), while C_t (mg/L) represents the equilibrium concentration. V (L) refers to the volume of the initial solution, and m (g) denotes the mass of the SCPH adsorbent.

3. Results and discussion

3.1. Structural characterization

As depicted in Fig. 2, the SEM image reveals a distinctive two-dimensional layered structure of SCPH. This network-like arrangement offers several advantages, including the exposure of many binding sites and the facilitation of mass transfer, thereby enhancing the efficiency of lead removal during the contaminant remediation process. Moreover, the EDX results (Fig. 2) indicate the presence of C, O, and N elements within SCPH. The significantly higher nitrogen content observed in SCPH suggests successfully integrating chitosan, which contains abundant amino groups, into the SA hydrogel. Interestingly, the analysis also reveals a notable decrease in calcium (Ca) content and a substantial increase in lead (Pb) content within the hydrogels after adsorption, indicating the possibility of ion exchange during the adsorption process [21]. The elemental mapping results of SCPH loaded with Pb(II) (SCPH-Pb) (Fig. 2) demonstrate that the element Pb is uniformly distributed throughout the adsorbent, implying an even distribution of reactive groups, such as –OH and –COOH, across the adsorbent matrix. Additionally, the observed two-dimensional layered structure of SCPH-Pb, as evidenced by Fig. 2, remains unchanged mainly after adsorption, demonstrating the excellent mechanical stability of SCPH even under adsorption conditions.

From Fig. 3 it is evident that the characteristic absorption peaks of the SCPH are predominantly observed at 3,375; 2,938; 1,608 and 1,422 cm^{-1}, corresponding to the stretching vibrations of O–H (N–H), C–H stretching vibrations on saturated carbon, asymmetric and symmetric –COOH vibrations, as well as asymmetric and symmetric C=H vibrations, respectively [22]. Among them, the peaks at 3,375 cm^{-1} O–H (N–H) and 1,608 (1,030) cm^{-1} (C=O) correspond to the $–NH_2$ of CS and the –COOH of SA, respectively. The peak at 1,608 (1,030) cm^{-1} corresponds to the stretching vibration of C–O in the G unit of SA [23,24], providing evidence for the successful electrostatic aggregation of SA and CS to form SCH [25]. It is worth noting that, compared to SCH, the peaks corresponding to –COOH and –OH in SCPH are broader and more intense. This comparison suggests the possible formation of hydrogen bonds between the molecules [26], confirming the successful modification of PVA. The intensities of peaks associated with –OH and –COOH functional groups at 1,608 and 3,375 cm^{-1}, respectively, decreased upon adsorption of Pb(II) [21]. This indicates the successful Pb(II) adsorption by SCPH and suggests that the functional groups –OH and –COOH play a significant role in the adsorption process [15]. The FTIR analysis results affirm the successful synthesis of SCPH through a cross-linking reaction, wherein CS serves as an electrostatic polymer and PVA acts as a modifying agent.

Fig. 3b displays the XRD patterns of SCH, SCPH, and SCPH-Pb. Regarding structural integrity, the XRD pattern of the SCPH before and after adsorption did not change significantly, indicating remarkable stability of SCPH, as corroborated by the SEM analysis. The XRD analysis revealed a single broad peak in the SCPH, indicating its amorphous nature. This observation suggests an increase in the disorderliness of the spatial arrangement within the synthetic hydrogel, leading to a larger specific surface area. This increase in surface area, in turn, enhances the material's adsorption properties. Furthermore, a comparison between SCH and SCPH reveals a weakening and broadening of the peak in the 2θ = 10°–20° region in the latter. This alteration indicates that the presence of Pb(II) ions partially inhibits the effect on the crystallization of the sodium alginate hydrogel. This phenomenon suggests that SCPH achieves a successful molecular-level integration with Pb, as supported by previous research by Tally and Atassi [27].

The zeta potential holds paramount importance as its magnitude correlates with the stability of particle dispersion.

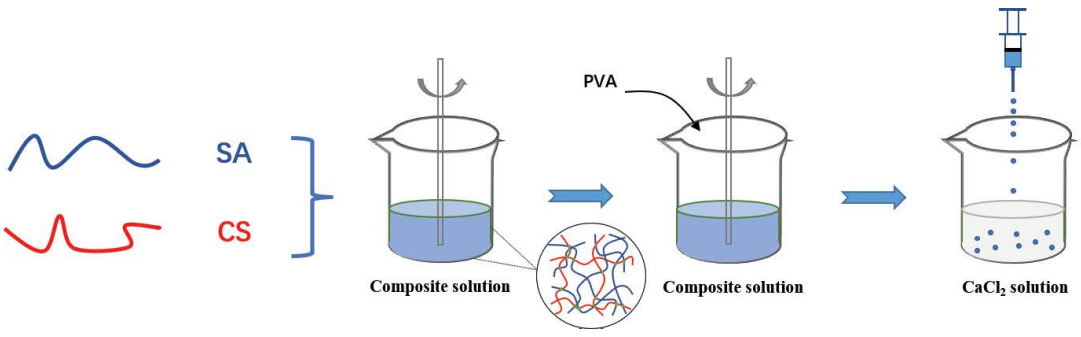

Fig. 1. Procedure for the synthesis of SCPH.

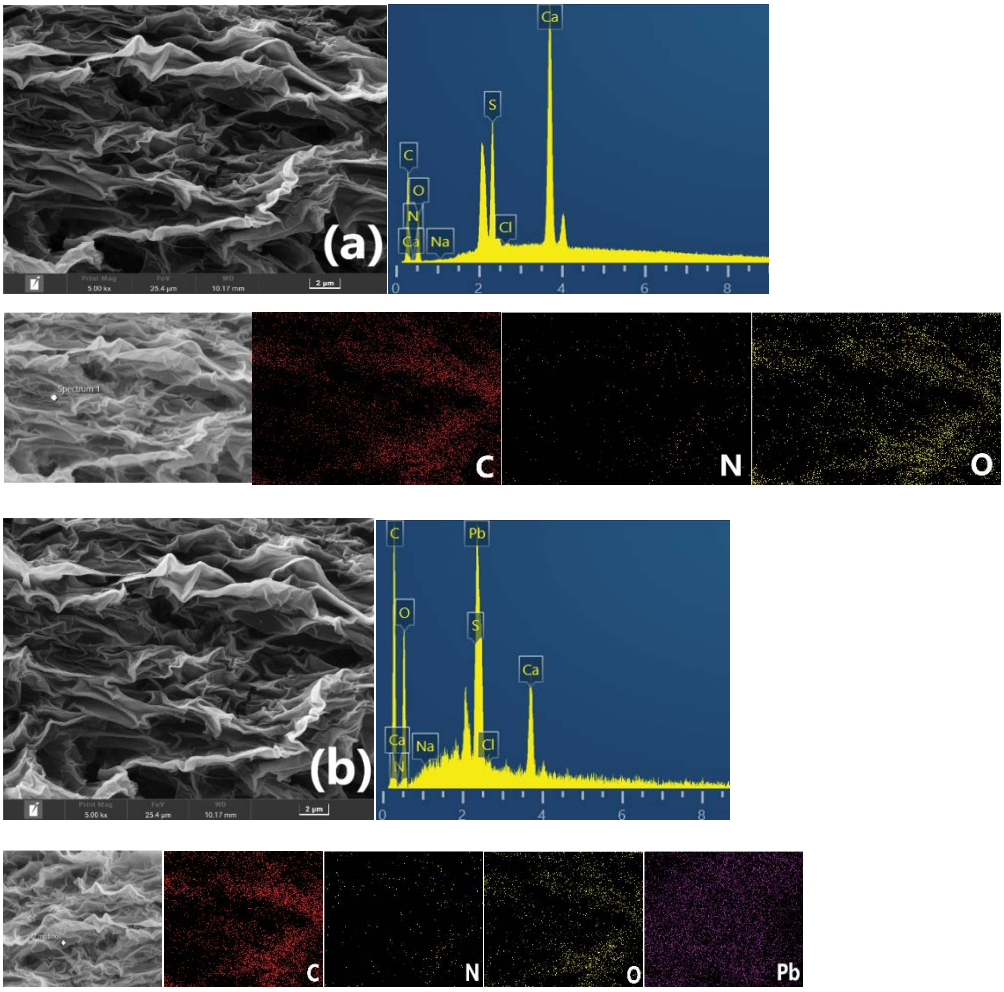

Fig. 2. Scanning electron microscopy images of (a) SCPH and (b) SCPH-Pb.

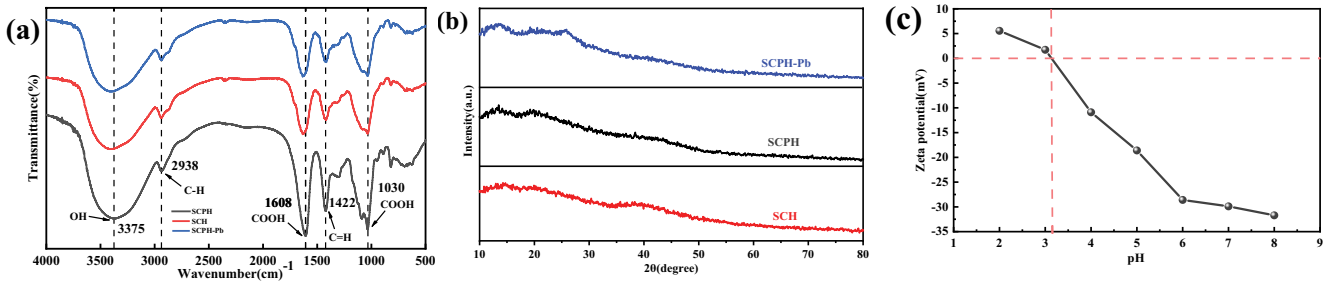

Fig. 3. (a) Fourier-transform infrared spectra of SCH, SCPH and SCPH-Pb, (b) X-ray diffraction patterns of SCH, SCPH and SCPH-Pb and (c) zeta potential of SCPH.

Smaller dispersed particles exhibit higher absolute zeta potential values, leading to enhanced system stability [28]. In this research, the zeta potential of powdered SCPH was evaluated at varying pH levels utilizing a particle size potentiostat (Malvern, Zetasizer Nano, China). Fig. 3c illustrates the zeta potential values of SCPH at various pH levels. Notably, the zeta potential curve demonstrates that SCPH carries a negative charge within the pH range of 3.5 to 8.0, while Pb(II) ions in the solution possess a positive direction. This electrostatic interaction demonstrates the electrostatic attraction effect of SCPH towards lead ions [29]. Interestingly, the zeta potential of the system under alkaline conditions is more significant in absolute value than under acidic conditions. This is because, under acidic conditions, H^+ affects the surface charge properties of the particles, resulting in a change in the zeta potential of the system. Under alkaline conditions, more and more OH^- is absorbed on the surface of particles, the negative charge on the surface of particles

increases, the repulsion between particles increases, the system zeta potential increases, and the dispersion system of adsorbents in water has a specific stability [30].

XPS was employed to further comprehend the adsorption mechanism of SCPH on Pb(II), and a comparative analysis was conducted. Fig. 4a displays the wide-scan XPS spectrum of SCPH and SCPH-Pb. Notably, a distinct peak emerged in SCPH-Pb, corresponding to the characteristic peak of Pb 4f. This finding unequivocally confirms the successful adsorption of lead ions onto SCPH. Moreover, the peak fitting analysis (Fig. 4b) reveals that, compared to Fig. 1, the signals at 143.68 and 138.83 eV in Fig. 2 corresponded to the Pb 4f 5/2 and Pb 4f 7/2 couple [29,31], respectively, providing further confirmation of Pb ion loading [29,31]. The emergence of Pb 4f doublet is due to the formation of PbC_2O_4 and –COO Pb [31], indicating chemical reactions between lead and oxygen on the SCPH surface [15]. In the C1s spectrum of SCPH (Fig. 4c), the peaks at binding energies of 284.68, 286.03, and 288.73 eV correspond to the C–C, C–O, and COO– functional groups, respectively [22,32]. Compared to the pre-adsorption state, the binding energies of SCPH after adsorption have shifted to 285.83 and 287.03 eV at C–O and COO– sites, respectively, indicating the presence of interactions between Pb(II) and –OH, –COOH [33,34]. These findings are consistent with the results obtained from FTIR. Fig. 4e also demonstrates the peaks of Ca 2p 1/2 and Ca 2p 3/2, corresponding to 350.88 and 347.58 eV, respectively. These peaks arise from the involvement of Ca(II) with the COO– groups on the G unit of SA in cross-linking. The intensity of both Ca peaks diminished after adsorption, accompanied by a shift in the binding energy to 347.1 and 351.2 eV, respectively [21]. This change indicates an ion exchange reaction between lead and calcium ions may occur. In conclusion, we can infer that the adsorption mechanism of SCPH on Pb(II) involves complexation processes and ion exchange.

3.2. Comparison of SH, SCH, and SCPH adsorption effects

The morphological characteristics and adsorption performance of the three materials are illustrated in Fig. 5. It can be seen that SCPH exhibits a flocculent hydrogel

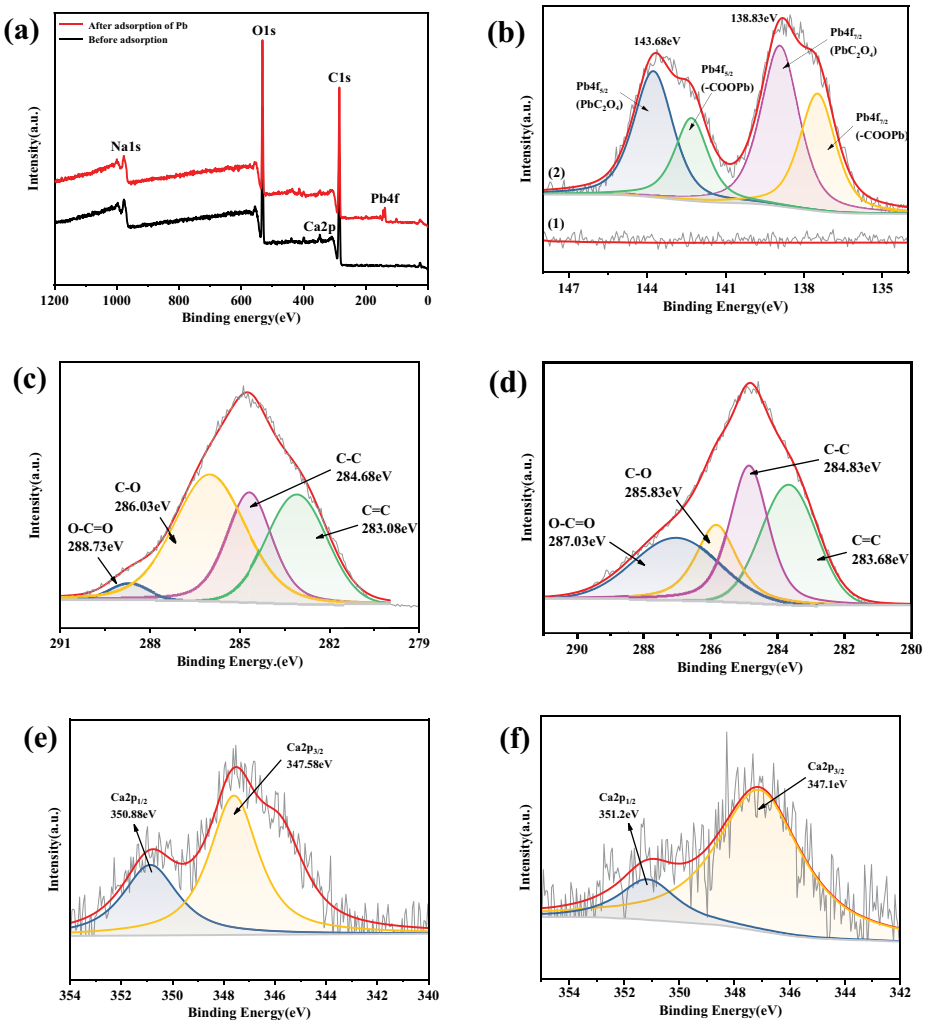

Fig. 4. (a) X-ray photoelectron spectroscopy full spectrum of SCPH and SCPH-Pb, (b) the Pb 4f spectra of SCPH (1) and SCPH-Pb (2), the C 2p spectra of SCPH (c) and SCPH-Pb (d) and the Ca 2p spectra of SCPH (e), and SCPH-Pb (f).

structure with a significantly enhanced specific surface area. Remarkably, SCPH displayed the highest adsorption capacity among the three materials, affirming the successful synthesis of the SCPH composite hydrogel.

3.3. Adsorption of Pb(II) with SCPH

3.3.1. Effect of SCPH dosage

The results are presented in Fig. 6a. It is evident that an increment in the adsorbent dosage leads to a notable enhancement in the removal rate while concurrently causing a decline in adsorption capacity. Subsequent elevations in the adsorbent dosage resulted in comparable removal rates, albeit with a continued reduction in sorption capacity. This is due to the too-low Pb(II) concentration and an excessive amount of adsorbent, resulting in the wastage of many unoccupied active adsorption sites [21]. Consequently, an accumulation of adsorbent impedes the attainment of saturation adsorption, thereby diminishing the adsorbent's overall utilization [21].

3.3.2. Effect of temperature

We investigated the impact of the temperature of SCPH on the adsorption of Pb(II) ions, as depicted in Fig. 6b. Our findings revealed that with the increase in temperature, the Q_t escalated from 111.24 mg/g (288 K) to 143.475 mg/g (313 K). The adsorption reaction was depicted as an energy-consuming [35] and endothermic process [36].

3.3.3. Effect of pH

Understanding the pH-dependent adsorption behavior of heavy metal ions in aqueous solutions is crucial for designing efficient adsorbents [37]. The results are depicted in Fig. 6c. As the pH value of the Pb(II) solution increases, the removal efficiency of hydrogel for Pb(II) increases from

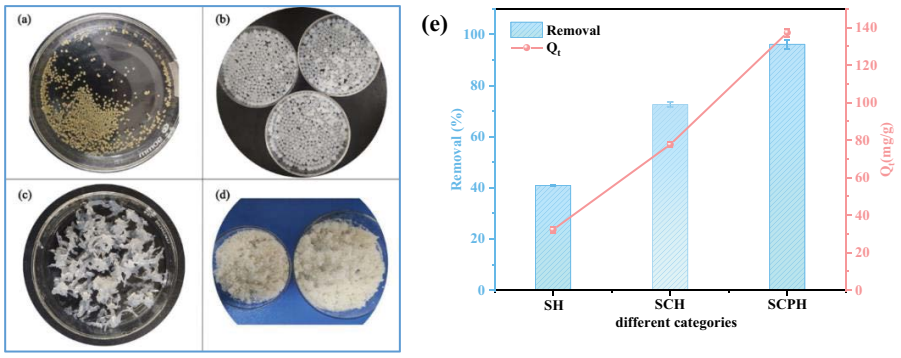

Fig. 5. (a) SH, (b) SCH, (c) SCPH (without drying), (d) SCPH (after freeze-drying), and (e) comparison of removal ratio of Pb(II) onto different hydrogels under same conditions.

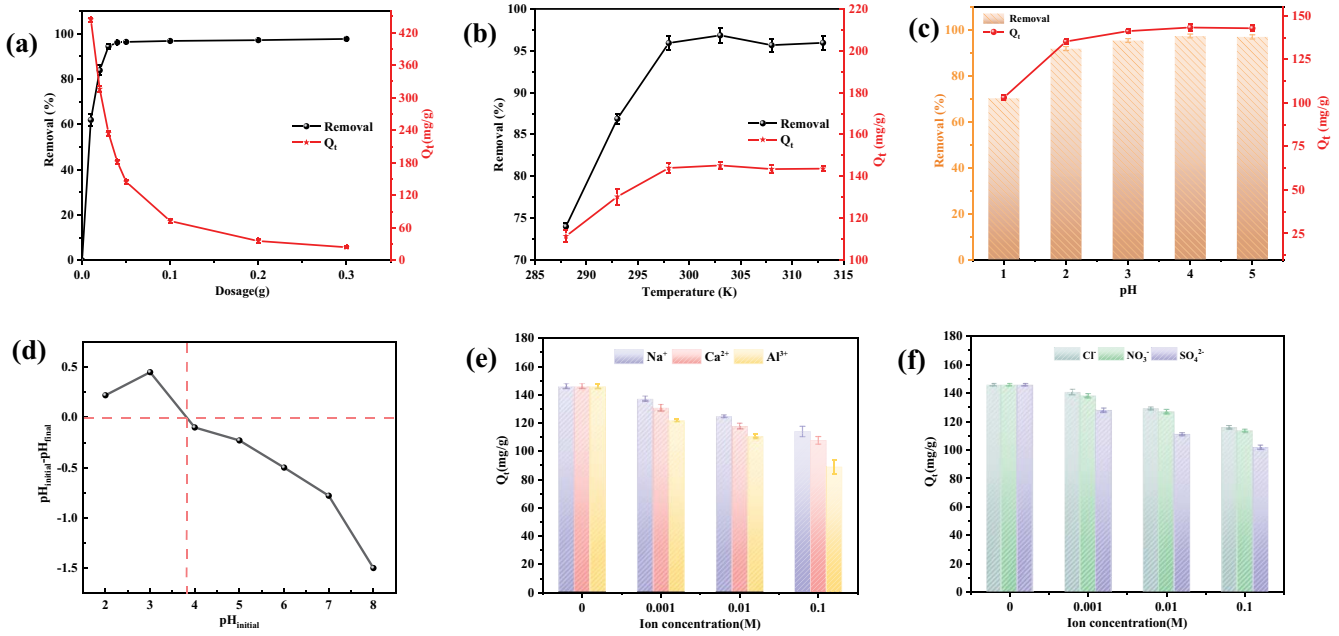

Fig. 6. Effect of (a) absorbent dosage, (b) temperature, and (c) pH on the adsorption of Pb(II) onto SCPH, (d) pH_{pzc} of SCPH; the effect of cations (e) and anions (f) on Pb(II) adsorption by SCPH.

69.56% to 96.07%, and the adsorption capacity increases from 104.34 to 144.78 mg/g, and then begins to decrease to 144.105 mg/g. The hydrogel's surface charge, modulated through protonation of –COOH functional groups [38], is important in determining the active adsorption sites and lead ion removal efficiency. We observed that the negatively charged surface facilitated the electrostatic attraction between Pb(II) ions and the hydrogel, enhancing adsorption performance. Conversely, excess H^+ ions in the solution competed with Pb(II) ions for adsorption sites, diminishing the adsorption capacity [39]. Precipitation of lead ions at high pH values was also observed, highlighting the importance of pH control for accurately determining adsorption capacity [40]. Furthermore, as depicted in Fig. 6d, the pH at the point of zero charge (pH_{pzc}) for SCPH fell within the range of 3–4. The adsorption of cationic Pb(II) by SCPH was found to intensify as the pH increased. This effect was attributed to the reduction in repulsive forces between the adsorbent and the adsorbate surface. Under the present experimental conditions, the adsorbent surface showed a weak negative charge, which indicated that the adsorption of Pb(II) by SCPH was not only by electrostatic gravitational force but also might be affected by various reaction mechanisms. In summary, combined with the results of zeta potential analysis, the solution pH four was selected as the subsequent adsorption experimental condition of SCPH.

3.3.4. Effect of coexisting ions

To comprehend the influence of coexisting ions on the removal of Pb(II) by SCPH, we conducted an investigation into the effects of cations like Ca^{2+} and Na^+ as well as anions such as Cl^- and NO_3^-, which are commonly found in water, on the performance of SCPH for the removal of Pb(II). As shown in Fig. 6, Na^+ and Ca^{2+} had almost no significant effect on the reduction of Pb(II). The adsorption capacity of SCPH was maintained above 110 mg/g regardless of Na^+ or Ca^{2+} concentration of 0.001 M or 0.1 M. In contrast, the effect was relatively significant in the presence of Al^{3+}. This may be because some active sites (containing N^-/O^-groups) with lone-pair electrons can also share electrons with metal cations (Ca^{2+} and Al^{3+}) to form metal complexes, which leads to a decrease in the adsorption of Pb(II) [41]. Na^+ has a much lower valence and a relatively small ionic radius, which may be the reason for its lesser influence on adsorption capacity [42]. For coexisting anions, their adsorption capacity on SCPH was only slightly affected due to partial occupation of adsorption sites [43].

3.3.5. Adsorption kinetics

In practical applications, reaction time is also crucial for the adsorption process of hydrogels. As presented in Fig. 7a, within the first 15 min, the absorption rate of the hydrogel is rapid, with over 90% of the adsorption process occurring within this time frame. Subsequently, the adsorption rate gradually increased until it reached equilibrium. The initial rapid adsorption might be attributed to the abundant active sites on the surface of SCPH, facilitating easy contact with Pb(II) [44]. However, as the adsorption process proceeds, the available active sites on SCPH become limited, resulting in a slower increase in adsorption capacity [45], eventually

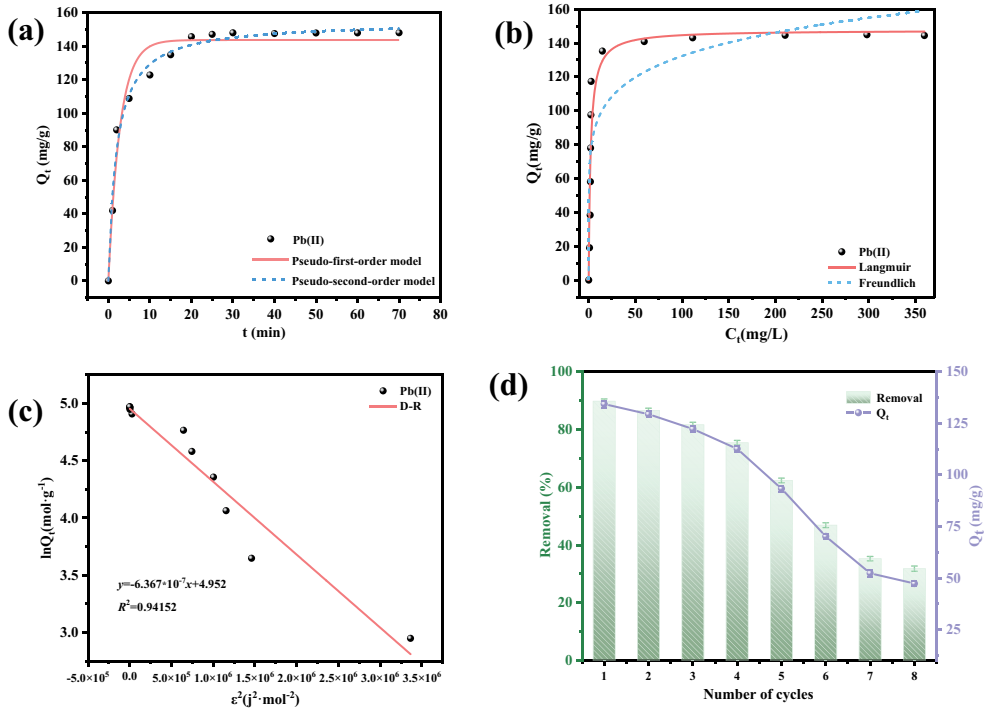

Fig. 7. (a) Effect of reaction time on the adsorption of Pb(II) onto SCPH, (b) the adsorption isotherms of Pb(II) onto SCPH, (c) Dubinin–Radushkevich isotherm plots obtained for the adsorption of Pb(II) onto SCPH, and (d) adsorption–desorption cycle for Pb(II) removal by SCPH (contact time = 1h).

leading to equilibrium. When reaching adsorption equilibrium, the adsorption capacity of SCPH is 147.93 mg/g. The pseudo-first-order [46] and pseudo-second-order [47] models were applied to analyze the adsorption behavior, as expressed by Eqs. (3) [48,49] and (4) [50,51]:

$$\log\left(Q_t - Q\right) = \log Q_t - \frac{k_a}{2.303}t \tag{3}$$

$$\frac{t}{Q} = \frac{1}{k_b Q_t^2} + \frac{1}{Q_t}t \tag{4}$$

where t (min), Q (mg/g), k_a (min^{-1}), and k_b (g/mg·min) represent time, corresponding adsorption amount, pseudo-first-order model rate constant, and pseudo-second-order model rate constant, respectively. The results of the curve fitting are presented in Fig. 7a.

Table 1 presents the experimental results and the theoretically calculated adsorption quantities, which indicate that the adsorption process followed the pseudo-second-order model, suggesting that chemical adsorption [52] was the predominant mechanism [53]. Physical adsorption [24] and electrostatic attraction also contributed to the overall adsorption process, as confirmed by the fit of the data and the high R^2 values obtained.

3.3.6. Adsorption isotherms

As presented in Fig. 7b, the fitting was performed using the Langmuir [54] and Freundlich isotherm model [55,56]. These models were expressed by Eqs. (5)–(7) [57,58].

Langmuir:

$$Q_t = \frac{Q_{\max} K_1 C_t}{1 + K_1 C_t} \tag{5}$$

$$R_1 = \frac{1}{1 + K_1 C_0} \tag{6}$$

Freundlich:

$$Q_t = K_2 C_t^{1/n} \tag{7}$$

where C_0 (mg/L), C_t (mg/L), Q_t (mg/g), and $Q_{\max}$ (mg/g) represent the initial concentration, equilibrium concentration, equilibrium adsorption capacity, and maximum adsorption capacity, respectively. The Langmuir constant K_1, Freundlich constant K_2, and n are associated with free energy, adsorption capacity, and adsorption intensity, respectively. The equilibrium parameter R_1 reflects the isotherm type.

The obtained fitted parameters are summarized in Table 2. It is worth noting that the Langmuir model exhibited a significantly higher correlation coefficient (R^2 = 0.9974) in comparison to the Freundlich model (R^2 = 0.7477), underscoring its superior fitting capability. These findings suggest that the monolayer adsorption process of Pb(II) onto SCPH follows the Langmuir isotherm model [59].

The Dubinin–Radushkevich (D-R) isothermal adsorption model is commonly used to describe the adsorption process and mechanism of porous materials [60]. The expressions for the D-R isothermal adsorption model are given in Eqs. (8)–(10) [60].

$$\ln Q_t = \ln Q_{\max} - \beta\varepsilon^2 \tag{8}$$

$$\varepsilon = RT\ln\left(1 + \frac{1}{C_t}\right) \tag{9}$$

$$E = \frac{1}{\sqrt{2\beta}} \tag{10}$$

where β (mol^2/kJ^2) is the D-R isothermal adsorption model constant, ε is the Polanyi adsorption potential, and R (8.314 J/mol·K) is the ideal gas constant.

Based on the fitted straight line between $\ln Q_t$ and ε^2 (Fig. 7c), $Q_{\max}$ and β could be calculated. β could be further utilized to calculate the mean adsorption-free energy (E, kJ/mol). The calculated average adsorption free energy (E) was 8.023 kJ/mol, which was in the range of 8–16 kJ/mol, indicating that the adsorption of Pb(II) in water by SCPH was mainly chemisorption [61]. This is consistent with the conclusion obtained from the above adsorption kinetics study.

The theoretical maximum adsorption capacity of SCPH for Pb(II) is 147.64 mg/g, and experimentally obtained,

Table 1
Kinetic parameters of Pb(II) adsorption onto SCPH

SCPH	Pseudo-first-order fit			Pseudo-second-order fit		
	Q_t	K_a	R^2	Q_t	K_b	R^2
Pb(II)	143.669	0.0449	0.96559	154.695	0.00327	0.98567

Table 2
Parameters of the Langmuir isotherm model, Freundlich isotherm model, and Dubinin–Radushkevich model for adsorption of Pb(II) onto SCPH

SCPH	Langmuir			Freundlich			Dubinin–Radushkevich		
	$Q_{\max}$	K	R^2	K	n	R^2	K_{DR}	E	R^2
Pb(II)	147.64	0.49	0.99753	68.33	6.97	0.7477	6.367×10^{-7}	8.023	0.94152

Table 3
Comparison of maximum adsorption of Pb(II) by composite adsorbents based on sodium alginate

Adsorbent	Contact time (h)	pH	Temperature (K)	Q_{max} (mg/g)	References
CCN/SA beads	3	5	298	335.4	[40]
Fe(III)-zeolite-SA beads	6.5	5.2	298	135.8	[63]
FeO/bentonite/AC/SA beads	24	4.5	298	74.18	[64]
SA-PAC-N-MAC	2	4.5	308	76.6	[65]
SA-DMSA	5	4	298	116.39	[66]
CCN/Fe_3O_4/SA	4	5	298	63.8	[31]
SA-CMC	18	5	310	77.3	[26]
Fe_3O_4-SA beads	3	4.8	298	98.8	[67]
NCS/SA beads	24	5	318	177.8	[68]
Alginate-UF beads	24	5	298	121.3	[19]
CTS/SA/Ca^{2+} PCDNH	8	3	298	175.6	[69]
SA-$CaCl_2$ beads	2	6	298	10	[70]
WSC-g-PKA/PVA	2	6	298	112	[68]
SA-PAM/GO	8	5.5	298	239.39	[71]
SA/PVA/PEO/ZSM-5 nanofiber	4	5.5	298	144	[72]
SA/CS/PVA (SCPH)	1.1	4	298	146	This work

CCN stands for chitosan/carboxylated nanocellulose. CCN is an acronym representing the combination of chitosan and carboxylated nanocellulose.

Q_{max} = 147.93 mg/g at 298 K. Table 3 compares the adsorption properties of the prepared SCPH with other similar composite hydrogels. Although the SCPH in this study was slightly inferior to the CCN/SA and SA-PAM/GO adsorbents, the adsorption capacity of SCPH was higher than that of other adsorbents, and the low cost and ability to be reutilized make the SCPH have a broad application prospect. Overall, the SCPH hydrogel in this study has the advantages of a simple preparation process, low cost, and reusability.

3.3.7. Recycling of SCPH

Fig. 7d shows the reusable performance of SCPH for Pb(II) adsorption. The results showed that after four adsorption–desorption cycle experiments, SCPH maintained a good removal effect (75.20% ± 0.2%) of Pb(II). At this time, the adsorption capacity of SCPH (112.6 ± 0.8 mg/g) was 76% of the maximum adsorption capacity (147.93 mg/g). This observation underscores the potential of SCPH as a proficient and reusable adsorbent for Pb(II). However, it is noteworthy that the adsorption capacity of SCPH for Pb(II) exhibited a substantial decline after the fourth cycle, reaching 47.34 mg/g after eight cycles. This phenomenon can likely be attributed to the stabilization of coordination bonds between the organic ligands within the SCPH hydrogel and Pb(II). Consequently, this stabilization reduced the availability of reactive hydroxyl groups within the hydrogel, thereby impeding the adsorption of Pb(II) [62].

4. Conclusion

This study presents a straightforward method for the fabrication of SCPH. The electrostatic polymerization of SA with CS and abundant reactive groups on both surfaces significantly facilitate the effective removal of Pb(II). Furthermore, introducing PVA in the SCH imparts enhanced selectivity and mechanical strength to the hydrogel because of the strong coordination group –OH. Compared to the original SH, the modified SCPH exhibits a distinct lamellar structure, increasing specific surface area. Through the analysis of characterization data, the mechanism by which SCPH removes Pb(II) is primarily through chemical adsorption, with ion exchange, surface hydroxyl groups, and carboxyl group complexation as the main factors, supported by electrostatic forces as a secondary form of physical adsorption. The SCPH can be easily prepared, exhibits rapid adsorption kinetics and high removal efficiency, and holds significant promise for removing Pb(II) from wastewater.

References

[1] G. Abdi, A. Alizadeh, S. Zinadini, G. Moradi, Removal of dye and heavy metal ion using a novel synthetic polyethersulfone nanofiltration membrane modified by magnetic graphene oxide/metformin hybrid, J. Membr. Sci., 552 (2018) 326–335.
[2] Y. Cao, W. Xiao, G. Shen, G. Ji, Y. Zhang, C. Gao, L. Han, Carbonization and ball milling on the enhancement of Pb(II) adsorption by wheat straw: competitive effects of ion exchange and precipitation, Bioresour. Technol., 273 (2019) 70–76.
[3] C. Xiong, S. Wang, W. Sun, Y. Li, Selective adsorption of Pb(II) from aqueous solution using nano-silica functionalized with diethanolamine: equilibrium, kinetic and thermodynamic, Microchem. J., 146 (2019) 270–278.
[4] M.E. Mahmoud, A.E.H. Abdou, G.M. Nabil, Facile microwave-assisted fabrication of nano-zirconium silicate-functionalized-3-aminopropyltrimethoxysilane as a novel adsorbent for superior removal of divalent ions, J. Ind. Eng. Chem., 32 (2015) 365–372.
[5] J. Hosseini, E.N. Zare, D. Ajloo, Experimental and theoretical calculation investigation on effective adsorption of lead(II) onto poly(aniline-*co*-pyrrole) nanospheres, J. Mol. Liq., 296 (2019) 111789, doi: 10.1016/j.molliq.2019.111789.

[6] Z. Karim, S. Claudpierre, M. Grahn, K. Oksman, A.P. Mathew, Nanocellulose based functional membranes for water cleaning: tailoring of mechanical properties, porosity and metal ion capture, J. Membr. Sci., 514 (2016) 418–428.
[7] W. Qin, G. Qian, H. Tao, J. Wang, J. Sun, X. Cui, Y. Zhang, X. Zhang, Adsorption of Hg(II) ions by PAMAM dendrimers modified attapulgite composites, React. Funct. Polym., 136 (2019) 75–85.
[8] V.K. Gupta, S. Agarwal, R. Ahmad, A. Mirza, J. Mittal, Sequestration of toxic congo red dye from aqueous solution using eco-friendly guar gum/activated carbon nanocomposite, Int. J. Biol. Macromol., 158 (2020) 1310–1318.
[9] I. Anastopoulos, A. Mittal, M. Usman, J. Mittal, G. Yu, A. Núñez-Delgado, M. Kornaros, A review on halloysite-based adsorbents to remove pollutants in water and wastewater, J. Mol. Liq., 269 (2018) 855–868.
[10] U.K. Sahu, S. Sahu, S.S. Mahapatra, R.K. Patel, Cigarette soot activated carbon modified with Fe_3O_4 nanoparticles as an effective adsorbent for As(III) and As(V): material preparation, characterization and adsorption mechanism study, J. Mol. Liq., 243 (2017) 395–405.
[11] V. Kumar, P. Saharan, A.K. Sharma, A. Umar, I. Kaushal, A. Mittal, Y. Al-Hadeethi, B. Rashad, Silver doped manganese oxide-carbon nanotube nanocomposite for enhanced dye-sequestration: isotherm studies and RSM modeling approach, Ceram. Int., 46 (2020) 10309–10319.
[12] I.M. Kenawy, M.A.H. Hafez, M.A. Ismail, M.A. Hashem, Adsorption of Cu(II), Cd(II), Hg(II), Pb(II) and Zn(II) from aqueous single metal solutions by guanyl-modified cellulose, Int. J. Biol. Macromol., 107 (2018) 1538–1549.
[13] I. Anastopoulos, I. Pashalidis, A.G. Orfanos, I.D. Manariotis, T. Tatarchuk, L. Sellaoui, A. Bonilla-Petriciolet, A. Mittal, A. Núñez-Delgado, Removal of caffeine, nicotine and amoxicillin from (waste)waters by various adsorbents. A review, J. Environ. Manage., 261 (2020) 110236, doi: 10.1016/j.jenvman.2020.110236.
[14] F. Karkeh-Abadi, S. Saber-Samandari, S. Saber-Samandari, The impact of functionalized CNT in the network of sodium alginate-based nanocomposite beads on the removal of Co(II) ions from aqueous solutions, J. Hazard. Mater., 312 (2016) 224–233.
[15] X. Xu, X.-k. Ouyang, L.-Y. Yang, Adsorption of Pb(II) from aqueous solutions using crosslinked carboxylated chitosan/carboxylated nanocellulose hydrogel beads, J. Mol. Liq., 322 (2021) 114523, doi: 10.1016/j.molliq.2020.114523.
[16] H.V. Sæther, H.K. Holme, G. Maurstad, O. Smidsrød, B.T. Stokke, Polyelectrolyte complex formation using alginate and chitosan, Carbohydr. Polym., 74 (2008) 813–821.
[17] Y. Chen, X. Yan, J. Zhao, H. Feng, P. Li, Z. Tong, Z. Yang, S. Li, J. Yang, S. Jin, Preparation of the chitosan/poly(glutamic acid)/alginate polyelectrolyte complexing hydrogel and study on its drug releasing property, Carbohydr. Polym., 191 (2018) 8–16.
[18] S. Thakur, B. Sharma, A. Verma, J. Chaudhary, S. Tamulevicius, V.K. Thakur, Recent progress in sodium alginate-based sustainable hydrogels for environmental applications, J. Cleaner Prod., 198 (2018) 143–159.
[19] P. Qu, Y. Li, H. Huang, J. Chen, Z. Yu, J. Huang, H. Wang, B. Gao, Urea formaldehyde modified alginate beads with improved stability and enhanced removal of Pb^{2+}, Cd^{2+}, and Cu^{2+}, J. Hazard. Mater., 396 (2020) 122664, doi: 10.1016/j.jhazmat.2020.122664.
[20] C. Liu, A. Omer, X.-k. Ouyang, Adsorptive removal of cationic methylene blue dye using carboxymethyl cellulose/k-carrageenan/activated montmorillonite composite beads: isotherm and kinetic studies, Int. J. Biol. Macromol., 106 (2018) 823–833.
[21] Z.-H. Hu, A.M. Omer, X.k. Ouyang, D. Yu, Fabrication of carboxylated cellulose nanocrystal/sodium alginate hydrogel beads for adsorption of Pb(II) from aqueous solution, Int. J. Biol. Macromol., 108 (2018) 149–157.
[22] W. Luo, Z. Bai, Y. Zhu, Fast removal of Co(II) from aqueous solution using porous carboxymethyl chitosan beads and its adsorption mechanism, RSC Adv., 8 (2018) 13370–13387.
[23] D. Tahtat, M. Mahlous, S. Benamer, A.N. Khodja, H. Oussedik-Oumehdi, F. Laraba-Djebari, Oral delivery of insulin from alginate/chitosan crosslinked by glutaraldehyde, Int. J. Biol. Macromol., 58 (2013) 160–168.
[24] X. Guan, B. Zhang, D. Li, M. He, Q. Han, J. Chang, Remediation and resource utilization of chromium(III)-containing tannery effluent based on chitosan-sodium alginate hydrogel, Carbohydr. Polym., 284 (2022) 119179, doi: 10.1016/j.carbpol.2022.119179.
[25] C.B. Godiya, X. Cheng, D. Li, Z. Chen, X. Lu, Carboxymethyl cellulose/polyacrylamide composite hydrogel for cascaded treatment/reuse of heavy metal ions in wastewater, J. Hazard. Mater., 364 (2019) 28–38.
[26] H. Ren, Z. Gao, D. Wu, J. Jiang, Y. Sun, C. Luo, Efficient Pb(II) removal using sodium alginate–carboxymethyl cellulose gel beads: preparation, characterization, and adsorption mechanism, Carbohydr. Polym., 137 (2016) 402–409.
[27] M. Tally, Y. Atassi, Synthesis and characterization of pH-sensitive superabsorbent hydrogels based on sodium alginate-g-poly(acrylic acid-co-acrylamide) obtained via an anionic surfactant micelle templating under microwave irradiation, Polym. Bull., 73 (2016) 3183–3208.
[28] S. Sekowski, E. Olchowik-Grabarek, W. Wieckowska, A. Veiko, L. Oldak, E. Gorodkiewicz, E. Karamov, N. Abdulladjanova, S. Mavlyanov, E. Lapshina, I.B. Zavodnik, M. Zamaraeva, Spectroscopic, zeta-potential and surface plasmon resonance analysis of interaction between potential anti-HIV tannins with different flexibility and human serum albumin, Colloids Surf., B, 194 (2020) 111175, doi: 10.1016/j.colsurfb.2020.111175.
[29] W. Zhao, D. Liu, Q. Feng, Enhancement of salicylhydroxamic acid adsorption by Pb(II) modified hemimorphite surfaces and its effect on floatability, Miner. Eng., 152 (2020) 106373, doi: 10.1016/j.mineng.2020.106373.
[30] M. Walters, S. Al Aani, P.P. Esteban, P.M. Williams, D.L. Oatley-Radcliffe, Laser Doppler electrophoresis and electro-osmotic flow mapping for the zeta potential measurement of positively charged membrane surfaces, Chem. Eng. Res. Des., 159 (2020) 468–476.
[31] J. Lu, R.-N. Jin, C. Liu, Y.-F. Wang, X.-k. Ouyang, Magnetic carboxylated cellulose nanocrystals as adsorbent for the removal of Pb(II) from aqueous solution, Int. J. Biol. Macromol., 93 (2016) 547–556.
[32] L. Fan, Y. Lu, L.-Y. Yang, F. Huang, X.-k. Ouyang, Fabrication of polyethyleneimine-functionalized sodium alginate/cellulose nanocrystal/polyvinyl alcohol core-shell microspheres ((PVA/SA/CNC)@PEI) for diclofenac sodium adsorption, J. Colloid Interface Sci., 554 (2019) 48–58.
[33] M. Zhang, Q. Yin, X. Ji, F. Wang, X. Gao, M. Zhao, High and fast adsorption of Cd(II) and Pb(II) ions from aqueous solutions by a waste biomass-based hydrogel, Sci. Rep., 10 (2020) 1–13.
[34] R. Jain, D. Dominic, N. Jordan, E.R. Rene, S. Weiss, E.D. van Hullebusch, R. Hübner, P.N. Lens, Preferential adsorption of Cu in a multi-metal mixture onto biogenic elemental selenium nanoparticles, Chem. Eng. J., 284 (2016) 917–925.
[35] S.A. Ali, O.C.S. Al Hamouz, N.M. Hassan, Novel cross-linked polymers having pH-responsive amino acid residues for the removal of Cu^{2+} from aqueous solution at low concentrations, J. Hazard. Mater., 248 (2013) 47–58.
[36] R.M. Ali, H.A. Hamad, M.M. Hussein, G.F. Malash, Potential of using green adsorbent of heavy metal removal from aqueous solutions: adsorption kinetics, isotherm, thermodynamic, mechanism and economic analysis, Ecol. Eng., 91 (2016) 317–332.
[37] H. Ren, Z. Gao, D. Wu, J. Jiang, Y. Sun, C. Luo, Efficient Pb(II) removal using sodium alginate–carboxymethyl cellulose gel beads: preparation, characterization, and adsorption mechanism, Carbohydr. Polym., 137 (2016) 402–409.
[38] Q. Zeng, Y. Huang, L. Huang, L. Hu, W. Sun, H. Zhong, Z. He, High adsorption capacity and super selectivity for Pb(II) by a novel adsorbent: nano humboldtine/almandine composite prepared from natural almandine, Chemosphere, 253 (2020) 126650, doi: 10.1016/j.chemosphere.2020.126650.

[39] J. Li, Z. Xu, W. Wu, Y. Jing, H. Dai, G. Fang, Nanocellulose/poly(2-(dimethylamino)ethyl methacrylate) interpenetrating polymer network hydrogels for removal of Pb(II) and Cu(II) ions, Colloids Surf., A, 538 (2018) 474–480.
[40] J. Ma, M. Zhang, M. Ji, L. Zhang, Z. Qin, Y. Zhang, L. Gao, T. Jiao, Magnetic graphene oxide-containing chitosan-sodium alginate hydrogel beads for highly efficient and sustainable removal of cationic dyes, Int. J. Biol. Macromol., 193 (2021) 2221–2231.
[41] Y. Huang, H. Wu, T. Shao, X. Zhao, H. Peng, Y. Gong, H. Wan, Enhanced copper adsorption by DTPA-chitosan/alginate composite beads: mechanism and application in simulated electroplating wastewater, Chem. Eng. J., 339 (2018) 322–333.
[42] Y. Wen, Z. Tang, Y. Chen, Y. Gu, Adsorption of Cr(VI) from aqueous solutions using chitosan-coated fly ash composite as biosorbent, Chem. Eng. J., 175 (2011) 110–116.
[43] S. Bao, W. Yang, Y. Wang, Y. Yu, Y. Sun, K. Li, PEI grafted amino-functionalized graphene oxide nanosheets for ultrafast and high selectivity removal of Cr(VI) from aqueous solutions by adsorption combined with reduction: behaviors and mechanisms, Chem. Eng. J., 399 (2020) 125762, doi: 10.1016/j.cej.2020.125762.
[44] D.-M. Guo, Q.-D. An, Z.-Y. Xiao, S.-R. Zhai, D.-J. Yang, Efficient removal of Pb(II), Cr(VI) and organic dyes by polydopamine modified chitosan aerogels, Carbohydr. Polym., 202 (2018) 306–314.
[45] H. Zhao, X.-K. Ouyang, L.-Y. Yang, Adsorption of lead ions from aqueous solutions by porous cellulose nanofiber–sodium alginate hydrogel beads, J. Mol. Liq., 324 (2021) 115122, doi: 10.1016/j.molliq.2020.115122.
[46] Z.-H. Hu, Y.F. Wang, A.M. Omer, X.k. Ouyang, Fabrication of ofloxacin imprinted polymer on the surface of magnetic carboxylated cellulose nanocrystals for highly selective adsorption of fluoroquinolones from water, Int. J. Biol. Macromol., 107 (2018) 453–462.
[47] N. Wang, Y.-F. Wang, A.M. Omer, X.-k. Ouyang, Fabrication of novel surface-imprinted magnetic graphene oxide-grafted cellulose nanocrystals for selective extraction and fast adsorption of fluoroquinolones from water, Anal. Bioanal. Chem., 409 (2017) 6643–6653.
[48] X.-X. Liang, N. Wang, Y.-L. Qu, L.-Y. Yang, Y.-G. Wang, X.-K. Ouyang, Facile preparation of metal-organic framework (MIL-125)/chitosan beads for adsorption of Pb(II) from aqueous solutions, Molecules, 23 (2018) 1524, doi: 10.3390/molecules23071524.
[49] J.-P. Fan, T.-T. Yuan, X.-K. Xu, X.-H. Zhang, Y.-T. Cheng, J.-J. Luo, Preparation and characterization of mock strawberry-like aminopropyl-modified mesoporous silica for column chromatographic purification of paclitaxel in *Taxus* × *Media*, Chem. Eng. J., 359 (2019) 1509–1517.
[50] C. Liu, R.-N. Jin, X.-k. Ouyang, Y.-G. Wang, Adsorption behavior of carboxylated cellulose nanocrystal—polyethyleneimine composite for removal of Cr(VI) ions, Appl. Surf. Sci., 408 (2017) 77–87.
[51] J.-P. Fan, J.-X. Yu, X.-M. Yang, X.-H. Zhang, T.-T. Yuan, H.-L. Peng, Preparation, characterization, and application of multiple stimuli-responsive rattle-type magnetic hollow molecular imprinted poly(ionic liquids) nanospheres (Fe_3O_4@void@PILMIP) for specific recognition of protein, Chem. Eng. J., 337 (2018) 722–732.
[52] J. Xiong, D. Zhang, H. Lin, Y. Chen, Amphiprotic cellulose mediated graphene oxide magnetic aerogels for water remediation, Chem. Eng. J., 400 (2020) 125890, doi: 10.1016/j.cej.2020.125890.
[53] Z.-H. Hu, A.M. Omer, X.k. Ouyang, D. Yu, Fabrication of carboxylated cellulose nanocrystal/sodium alginate hydrogel beads for adsorption of Pb(II) from aqueous solution, Int. J. Biol. Macromol., 108 (2018) 149–157.
[54] N. Wang, X.-K. Ouyang, L.-Y. Yang, A.M. Omer, Fabrication of a magnetic cellulose nanocrystal/metal-organic framework composite for removal of Pb(II) from water, ACS Sustainable Chem. Eng., 5 (2017) 10447–10458.
[55] Y.-F. Wang, Y.-G. Wang, X.-K. Ouyang, L.-Y. Yang, Surface-imprinted magnetic carboxylated cellulose nanocrystals for the highly selective extraction of six fluoroquinolones from egg samples, ACS Appl. Mater. Interfaces, 9 (2017) 1759–1769.
[56] J.P. Fan, F.Y. Zhang, X.M. Yang, X.H. Zhang, Y.H. Cao, H.L. Peng, Preparation of a novel super macroporous molecularly imprinted cryogel membrane with a specific ionic liquid for protein recognition and perm selectivity, J. Appl. Polym. Sci., 135 (2018) 46740, doi: 10.1002/app.46740.
[57] D. Gusain, V. Srivastava, Y.C. Sharma, Kinetic and thermodynamic studies on the removal of Cu(II) ions from aqueous solutions by adsorption on modified sand, J. Ind. Eng. Chem., 20 (2014) 841–847.
[58] H.N. Tran, S.-J. You, H.-P. Chao, Thermodynamic parameters of cadmium adsorption onto orange peel calculated from various methods: a comparison study, J. Environ. Chem. Eng., 4 (2016) 2671–2682.
[59] Z. Liu, G. Chen, F. Zhou, J. Huang, Imidazolium salt incorporated poly(N-vinylimidazole-co-ethylene glycol dimethacrylate) for efficient adsorption of Congo red and Hg^{2+} from aqueous solution, J. Chem. Eng. Data, 64 (2019) 2627–2633.
[60] F.A. Ngwabebhoh, M. Gazi, A.A. Oladipo, Adsorptive removal of multi-azo dye from aqueous phase using a semi-IPN superabsorbent chitosan-starch hydrogel, Chem. Eng. Res. Des., 112 (2016) 274–288.
[61] J. Luo, X. Luo, C. Hu, J.C. Crittenden, J. Qu, Zirconia (ZrO_2) embedded in carbon nanowires via electrospinning for efficient arsenic removal from water combined with DFT studies, ACS Appl. Mater. Interfaces, 8 (2016) 18912–18921.
[62] Y. Foroutan, Ethnic or religious identities?: multicultural analysis in Australia from socio-demographic perspective, J. Ethnic Cultural Stud., 7 (2020) 1–19.
[63] M. Kragović, S. Pašalić, M. Marković, M. Petrović, B. Nedeljković, M. Momčilović, M. Stojmenović, Natural and modified zeolite—alginate composites. application for removal of heavy metal cations from contaminated water solutions, Minerals, 8 (2018) 11, doi: 10.3390/min8010011.
[64] R.R. Pawar, Lalhmunsiama, M. Kim, J.-G. Kim, S.-M. Hong, S.Y. Sawant, S.M. Lee, Efficient removal of hazardous lead, cadmium, and arsenic from aqueous environment by iron oxide modified clay-activated carbon composite beads, Appl. Clay Sci., 162 (2018) 339–350.
[65] T. Tripathy, H. Kolya, S. Jana, Selective lead(II) adsorption and flocculation characteristics of the grafted sodium alginate: a comparative study, J. Polym. Environ., 26 (2018) 926–937.
[66] Z. Wang, S. Wu, Y. Zhang, L. Miao, Y. Zhang, A. Wu, Preparation of modified sodium alginate aerogel and its application in removing lead and cadmium ions in wastewater, Int. J. Biol. Macromol., 157 (2020) 687–694.
[67] A. Bée, D. Talbot, S. Abramson, V. Dupuis, Magnetic alginate beads for Pb(II) ions removal from wastewater, J. Colloid Interface Sci., 362 (2011) 486–492.
[68] E.-h. Ablouh, A. Essaghraoui, N. Eladlani, M. Rhazi, M. Taourirte, Uptake of Pb(II) onto nanochitosan/sodium alginate hybrid beads: mechanism and kinetics study, Wate Environ. Res., 91 (2019) 239–249.
[69] S. Tang, J. Yang, L. Lin, K. Peng, Y. Chen, S. Jin, W. Yao, Construction of physically crosslinked chitosan/sodium alginate/calcium ion double-network hydrogel and its application to heavy metal ions removal, Chem. Eng. J., 393 (2020) 124728, doi: 10.1016/j.cej.2020.124728.
[70] C.-l. Zheng, Q.-r. Wang, G.-q. Geng, Z.-x. Wang, H. Zhuo, Adsorption of lead ions by a kind of MAL modified hydrogel beads, Trans. Nonferrous Met. Soc. China, 32 (2022) 2770–2786.
[71] H. Jiang, Y. Yang, Z. Lin, B. Zhao, J. Wang, J. Xie, A. Zhang, Preparation of a novel bio-adsorbent of sodium alginate grafted polyacrylamide/graphene oxide hydrogel for the adsorption of heavy metal ion, Sci. Total Environ., 744 (2020) 140653, doi: 10.1016/j.scitotenv.2020.140653.
[72] M. Talebi, S. Abbasizadeh, A.R. Keshtkar, Evaluation of single and simultaneous thorium and uranium sorption from water systems by an electrospun PVA/SA/PEO/HZSM5 nanofiber, Process Saf. Environ. Prot., 109 (2017) 340–356.